Impact of polarization observables and Bc→ on new physics explanations of the b→c anomaly

Blanke, Monika ; Crivellin, Andreas ; de Boer, Stefan ; Moscati, Marta ; Nierste, Ulrich ; Nišandžić, Ivan ; Kitahara, Teppei

Abstract: The combined analysis of the BABAR, Belle, and LHCb data on B→D , B→D∗ and Bc→J/Ψ decay observables shows evidence of physics beyond the Standard Model (SM). In this article, we study all the one- and two-dimensional scenarios which can be generated by adding a single new particle to the SM. We put special emphasis on the model-discriminating power of FL(D∗) and of the polarizations, and especially on the constraint from the branching fraction BR(Bc→). We critically review this constraint and do not support the aggressive limit of BR(Bc→)<10% used in some analyses. While the impact of FL(D∗) is currently still limited, the BR(Bc→) constraint has a significant impact: depending on whether one uses a limit of 60%, 30% or 10%, the pull for new physics (NP) in scalar operators changes drastically. More specifically, for a conservative 60% limit a scenario with scalar operators gives the best fit to data, while for an aggressive 10% limit this scenario is strongly disfavored and the best fit is obtained in a scenario in which only a left-handed vector operator is generated. We find a sum rule for the branching ratios of B→D , B→D∗ and Λb→Λc which holds for any NP contribution to the Wilson coefficients. This sum rule entails an enhancement of BR(Λb→Λc) over its SM prediction by (24±6)% for the current R(D(*)) data.

DOI: https://doi.org/10.1103/physrevd.99.075006

Impact of polarization observables and $B_c \to \tau\nu$ on new physics explanations of the $b \to c\tau\nu$ anomaly

Monika Blanke[*]
Institut für Kernphysik (IKP), Karlsruher Institut für Technologie (KIT), 76021 Karlsruhe, Germany
Institut für Theoretische Teilchenphysik (TTP), Karlsruher Institut für Technologie (KIT), 76131 Karlsruhe, Germany

Andreas Crivellin[†]
Paul Scherrer Institut, CH–5232 Villigen PSI, Switzerland

Stefan de Boer,[‡] Marta Moscati,[§] Ulrich Nierste,[‖] and Ivan Nišandžić[¶]
Institut für Theoretische Teilchenphysik (TTP), Karlsruher Institut für Technologie (KIT), 76131 Karlsruhe, Germany

Teppei Kitahara[**]
Institute for Advanced Research, Nagoya University, Furo-cho Chikusa-ku, Nagoya 464-8602, Japan; Kobayashi-Maskawa Institute for the Origin of Particles and the Universe, Nagoya University, Nagoya 464-8602, Japan
and Physics Department, Technion–Israel Institute of Technology, Haifa 3200003, Israel

(Received 4 December 2018; published 5 April 2019)

The combined analysis of the *BABAR*, Belle, and LHCb data on $B \to D\tau\nu$, $B \to D^*\tau\nu$ and $B_c \to J/\Psi\tau\nu$ decay observables shows evidence of physics beyond the Standard Model (SM). In this article, we study all the one- and two-dimensional scenarios which can be generated by adding a single new particle to the SM. We put special emphasis on the model-discriminating power of $F_L(D^*)$ and of the τ polarizations, and especially on the constraint from the branching fraction $\mathrm{BR}(B_c \to \tau\nu)$. We critically review this constraint and do not support the aggressive limit of $\mathrm{BR}(B_c \to \tau\nu) < 10\%$ used in some analyses. While the impact of $F_L(D^*)$ is currently still limited, the $\mathrm{BR}(B_c \to \tau\nu)$ constraint has a significant impact: depending on whether one uses a limit of 60%, 30% or 10%, the pull for new physics (NP) in scalar operators changes drastically. More specifically, for a conservative 60% limit a scenario with scalar operators gives the best fit to data, while for an aggressive 10% limit this scenario is strongly disfavored and the best fit is obtained in a scenario in which only a left-handed vector operator is generated. We find a sum rule for the branching ratios of $B \to D\tau\nu$, $B \to D^*\tau\nu$ and $\Lambda_b \to \Lambda_c\tau\nu$ which holds for any NP contribution to the Wilson coefficients. This sum rule entails an enhancement of $\mathrm{BR}(\Lambda_b \to \Lambda_c\tau\nu)$ over its SM prediction by $(24 \pm 6)\%$ for the current $\mathcal{R}(D^{(*)})$ data.

DOI: 10.1103/PhysRevD.99.075006

I. INTRODUCTION

Low-energy precision flavor observables probe new physics (NP) in a complementary way to direct searches for new particles at high energies. In this respect, tauonic B meson decays are an excellent window into NP: in combination with the well-studied B decays to light leptons ($\ell = \mu,\ e$) they test lepton flavor universality (LFU). Within the Standard Model (SM), LFU is only broken by the small Higgs Yukawa interactions and it manifests itself (to a very good approximation) only via the masses entering the phase space of the different decay modes.

The theory predictions for the individual semileptonic decay rates suffer from hadronic uncertainties related to the form factors and from parametric uncertainties stemming from the errors in the CKM elements (e.g., see Refs. [1–3] for recent reviews). However, in normalizing the branching ratios $\mathrm{BR}(B \to D^{(*)}\tau\nu)$ to $\mathrm{BR}(B \to D^{(*)}\ell\nu)$, $\ell = \mu, e$, and analogously also their counterparts for other b-flavored hadrons,

[*]monika.blanke@kit.edu
[†]andreas.crivellin@cern.ch
[‡]stefan.boer@kit.edu
[§]marta.moscati@kit.edu
[‖]ulrich.nierste@kit.edu
[¶]ivan.nisandzic@kit.edu
[**]teppeik@kmi.nagoya-u.ac.jp

$$\mathcal{R}(D^{(*)}) \equiv \mathrm{BR}(B \to D^{(*)}\tau\nu)/\mathrm{BR}(B \to D^{(*)}\ell\nu),$$
$$\mathcal{R}(J/\Psi) \equiv \mathrm{BR}(B_c \to J/\Psi\tau\nu)/\mathrm{BR}(B_c \to J/\Psi\ell\nu),$$
$$\mathcal{R}(\Lambda_c) \equiv \mathrm{BR}(\Lambda_b \to \Lambda_c\tau\nu)/\mathrm{BR}(\Lambda_b \to \Lambda_c\ell\nu), \quad (1)$$

the dependence on the CKM elements drops out and the uncertainties originating from the form factors are significantly reduced [4–7].

Experimentally, the *BABAR* Collaboration performed an analysis of $\mathcal{R}(D)$ and $\mathcal{R}(D^*)$ using the full available data set [8,9]. The same ratios were also measured by the Belle Collaboration [10–13], while the LHCb Collaboration has measured $\mathcal{R}(D^*)$ [14–16]. Combining these data, the HFLAV Collaboration [17] determines the ratios

$$\mathcal{R}(D) = 0.407 \pm 0.039 \pm 0.024,$$
$$\mathcal{R}(D^*) = 0.306 \pm 0.013 \pm 0.007. \quad (2)$$

Here, the first error is statistical and the second one is systematic. Comparing these measurements to the corresponding SM predictions [18–21]

$$\mathcal{R}_{\mathrm{SM}}(D) = 0.299 \pm 0.003,$$
$$\mathcal{R}_{\mathrm{SM}}(D^*) = 0.258 \pm 0.005, \quad (3)$$

reveals a tension at the level of 3.8σ [17].[1] This is also consistent with the previous evaluations of $\mathcal{R}(D)$ in Refs. [4,5,22,24,25] and of $\mathcal{R}(D^*)$ in Ref. [6].

The observed anomaly receives further support from the LHCb analysis of $\mathcal{R}(J/\Psi)$ [26] which also finds an experimental value significantly above the SM prediction. Unfortunately, the relevant form factors are poorly known in this case [27–29]. Hence we do not include this measurement in our analysis. For a discussion of NP effects in $\mathcal{R}(J/\psi)$, see Refs. [30,31].

For later use we further quote the SM prediction for the ratio $\mathcal{R}(\Lambda_c)$ [32]:

$$\mathcal{R}_{\mathrm{SM}}(\Lambda_c) = 0.33 \pm 0.01. \quad (4)$$

The Belle Collaboration has measured the τ polarization asymmetry along the longitudinal directions of the τ lepton in $B \to D^*\tau\nu$, defined as

$$P_\tau(D^*) = \frac{\Gamma(B \to D^*\tau^{\lambda=+1/2}\nu) - \Gamma(B \to D^*\tau^{\lambda=-1/2}\nu)}{\Gamma(B \to D^*\tau\nu)}, \quad (5)$$

where λ denotes the τ helicity, obtaining [12,13]

$$P_\tau(D^*) = -0.38 \pm 0.51^{+0.21}_{-0.16}. \quad (6)$$

[1]Recent discussions of long-distance electromagnetic effects in $\mathcal{R}(D)$ can be found in Refs. [22,23].

This observable turns out to be interesting for discriminating NP models, especially if the accuracy is improved in the future by the Belle II experiment.

Recently, the Belle Collaboration has also measured the longitudinal D^* polarization in $B \to D^*\tau\nu$, defined as

$$F_L(D^*) = \frac{\Gamma(B \to D_L^*\tau\nu)}{\Gamma(B \to D^*\tau\nu)}. \quad (7)$$

Like the τ polarization, also the D^* polarization can distinguish between different Lorentz structures; i.e., NP in scalar, tensor or vector operators affects the D^* polarization in a complementary way to the overall rate. The preliminary Belle result is [33]

$$F_L(D^*) = 0.60 \pm 0.08 \pm 0.035, \quad (8)$$

which agrees with the SM prediction of

$$F_{L,\mathrm{SM}}(D^*) = 0.46 \pm 0.04, \quad (9)$$

at the 1.5σ level [34]. Nonetheless, this result can still favor or disfavor specific NP scenarios.

Similarly, the τ polarization in $B \to D\tau\nu$ can provide information about the Lorentz structure of NP [4,7]. However, $P_\tau(D)$ has not been measured yet. The reason for this is that the τ is reconstructed in decay modes with at least one neutrino, and the missing energy blurs the information on the τ momentum. One can deal with this problem by considering differential decay distributions involving only kinematic variables of the *visible* final state particles, for instance the D and π energies, and the angle between the D and π tracks in the decay chain $B \to D\nu\tau[\to \pi\nu]$. These decay distributions have a high sensitivity to NP [4,7].

Furthermore, the B_c lifetime has a significant impact on possible NP solutions [35,36], because it constrains the yet unmeasured branching ratio $\mathrm{BR}(B_c \to \tau\nu)$. The lifetime measurement is very precise [37],

$$\tau(B_c) = (0.507 \pm 0.009)\ \mathrm{ps}, \quad (10)$$

while a theory prediction is quite challenging (we will return to this issue in detail later).

Even though many model independent analyses in this context have been performed [34,35,38–62], it is important to reconsider the situation in light of the recent $F_L(D^*)$ measurement and to critically revise and examine the treatment of the $B_c \to \tau\nu$ decay. Furthermore, we will highlight the future potential of the polarization observables $F_L(D^*)$, $P_\tau(D^*)$, and (the yet unmeasured) $P_\tau(D)$ to discriminate between different scenarios of NP. We will also highlight the interplay among $\mathcal{R}(D^{(*)})$ and $\mathcal{R}(\Lambda_c)$, where $\mathcal{R}(\Lambda_c)$ provides a consistency check of the measurements.

The paper is organized as follows. In Sec. II, we fix our notation for the relevant effective Hamiltonian. In Sec. III, we discuss theoretical and phenomenological aspects of $\mathrm{BR}(B_c \to \tau\nu)$ and list compact analytic formulas for the considered observables. In Sec. IV, we present our phenomenological studies in scenarios with one and two nonzero NP Wilson coefficients. The chosen scenarios correspond to the cases in which the NP coefficients are generated by the exchange of a single heavy spin-0 or spin-1 particle. Section V is devoted to the study of correlations between the ratios $\mathcal{R}(D^{(*)})$ and $\mathcal{R}(\Lambda_c)$ and the polarization observables $F_L(D^*)$ and $P_\tau(D^{(*)})$. Finally, we conclude in Sec. VI.

II. EFFECTIVE FIELD THEORY

We are interested in NP which is realized above the B meson mass scale. Especially in the case at hand, this is a reasonable assumption, since modifying a charged current obviously requires a new charged particle for which light masses are experimentally excluded. Therefore, we can integrate out the heavy degrees of freedom, and the SM as well as the NP physics contributions are parametrized by the effective Hamiltonian

$$\begin{aligned}\mathcal{H}_{\mathrm{eff}} = 2\sqrt{2}G_F V_{cb}[&(1+C_V^L)O_V^L + C_S^R O_S^R \\ &+ C_S^L O_S^L + C_T O_T],\end{aligned} \tag{11}$$

with

$$\begin{aligned}O_V^L &= (\bar{c}\gamma^\mu P_L b)(\bar{\tau}\gamma_\mu P_L \nu_\tau),\\ O_S^R &= (\bar{c}P_R b)(\bar{\tau}P_L \nu_\tau),\\ O_S^L &= (\bar{c}P_L b)(\bar{\tau}P_L \nu_\tau),\\ O_T &= (\bar{c}\sigma^{\mu\nu}P_L b)(\bar{\tau}\sigma_{\mu\nu}P_L \nu_\tau),\end{aligned} \tag{12}$$

where we assumed the absence of both (light) right-handed neutrinos,[2] and of NP couplings to the light lepton generations (as studied in Ref. [67]). Note that we have factored out the SM contribution such that all Wilson coefficients $C_{S,V,T}^{L,R}$ originate from NP only. Here we do not include a vector operator with a right-handed coupling to quarks, because such an operator (with the desired LFU violation) does not arise at the dimension-six level in the $\mathrm{SU}(2)_L$-invariant effective theory [68–70].

The Wilson coefficients in Eq. (11) depend on the renormalization scale. We will quote our results for the coefficients defined at the scale of the heavy NP particle, which we take as 1 TeV. The coefficients at the scale $\mu = m_b$ are related to those defined at 1 TeV as [71]

$$\begin{aligned}C_V^L(m_b) &= C_V^L(1\ \mathrm{TeV}),\\ C_S^R(m_b) &= 1.737 C_S^R(1\ \mathrm{TeV}),\\ \begin{pmatrix} C_S^L(m_b) \\ C_T(m_b)\end{pmatrix} &= \begin{pmatrix} 1.752 & -0.287 \\ -0.004 & 0.842\end{pmatrix}\begin{pmatrix} C_S^L(1\ \mathrm{TeV}) \\ C_T(1\ \mathrm{TeV})\end{pmatrix}.\end{aligned} \tag{13}$$

III. OBSERVABLES

While the theory predictions for $\mathcal{R}(D^{(*)})$ in Eq. (2) as well as the polarization observables like $F_L(D^*)$ in Eq. (8) are quite straightforward, the B_c lifetime constraint in Eq. (10) warrants some discussion. In principle, the decay width of $B_c \to \tau\nu$ places a powerful constraint on the scalar operators in Eq. (11). However, the branching ratio $\mathrm{BR}(B_c \to \tau\nu)$ has not been measured yet. Therefore, one only has the option of comparing the measured B_c lifetime with the theoretical calculations of Refs. [72–76]. In this way the authors of Ref. [36] have set an upper limit of 30% on the contribution from $B_c \to \tau\nu$ to the total B_c decay width. Furthermore, the authors of Ref. [77] even advocate that the NP contribution to $\mathrm{BR}(B_c \to \tau\nu)$ can be at most 10%.

A. Constraints from $\mathrm{BR}(B_c \to \tau\nu)$

For the estimate of $\mathrm{BR}(B_c \to \tau\nu) < 10\%$ from Ref. [77], LEP data on a mixture of $B_c \to \tau\nu$ and $B^- \to \tau\nu$ decays (with b quarks from Z boson decays) are used as an input. In order to extract information on $\mathrm{BR}(B_c \to \tau\nu)$ from these data one must know the probability f_c that a b quark hadronizes into a B_c meson. f_c is a small number, of the order of 10^{-2} or less. In Ref. [77] the ratio of the $b \to B_c$ and $b \to B_u$ fragmentation functions, f_c/f_u, is extracted from data accumulated at hadron colliders. As a first critical remark, we recall that fragmentation functions depend on the kinematics. In the case of the $b \to B_s$ and $b \to B_d$ fragmentation functions the LHCb Collaboration indeed finds evidence for a decrease of f_s/f_d with the transverse momentum p_T of the $B_{d,s}$ meson [78]. The authors of Ref. [77] infer f_c/f_u from an average of CMS and LHCb measurements of

$$R \equiv \frac{f_c}{f_u}\frac{\mathrm{BR}(B_c^- \to J/\psi\pi^-)}{\mathrm{BR}(B^- \to J/\psi K^-)}. \tag{14}$$

The individual measurements are [17,79,80]

$$\begin{aligned}R &= (4.8 \pm 0.5 \pm 0.6)\times 10^{-3} \quad [\mathrm{CMS}],\\ R &= (6.83 \pm 0.18 \pm 0.09)\times 10^{-3} \quad [\mathrm{LHCb}].\end{aligned} \tag{15}$$

[2]For studies of right-handed neutrino effects in $\mathcal{R}(D^{(*)})$, see [63–66].

Since CMS data are taken for $p_T > 15$ GeV while LHCb employs $0 < p_T < 20$ GeV, the data seemingly support a decrease of R and thereby of f_c/f_u with p_T, in qualitative agreement with the LHCb finding for f_s/f_d. Furthermore, the p-p collisions at CMS and LHCb or p-$\bar{p}$ collisions at the Tevatron produce B_c mesons through mechanisms which have no counterpart in Z decays: a prominent production process at hadron machines involves a $\bar{b}$ quark from one (anti)proton and a c quark from the other one, i.e., mechanisms involving heavy-quark parton distribution functions or gluon splittings into heavy-quark pairs. We therefore doubt that values for f_c/f_u extracted from Tevatron and LHC data can directly be used for Z peak analyses.

Moreover, even the 30% limit from Ref. [36] has to be taken with a grain of salt. Recall that the dominant contribution to the B_c decay rate comes from the decay of the charm quark within the B_c meson. The applicability of the calculational method (expansion in inverse powers of the heavy-quark masses combined with nonrelativistic QCD) to this charm decay is not clear and the result found in Ref. [74] exhibits a large dependence on the value of the charm mass, which moreover is not well defined in a leading-order QCD calculation. To constrain NP effects in the B_c lifetime the upper bound of the SM prediction $0.4\ \text{ps} \leq \tau(B_c) \leq 0.7\ \text{ps}$ [74] is relevant, because it corresponds to the smallest possible SM contribution to the total B_c decay width. Lowering the charm mass by only 0.05 GeV below the value of 1.4 GeV used as the lower limit in Ref. [74], the allowed NP contribution to the total B_c width increases to 40%. Taking into account all uncertainties the assumption of up to 60% room for NP in the B_c decay width is not too conservative. Therefore, we will show our results for three different limits on the $B_c \to \tau\nu$ branching ratio: 10%, 30%, and 60%.

B. Numerical formulas

The observables of interest are given by

$$\mathcal{R}(D) \simeq \mathcal{R}_{\rm SM}(D)\{|1+C_V^L|^2 + 1.54\text{Re}[(1+C_V^L)(C_S^{L*}+C_S^{R*})] + 1.09|C_S^L+C_S^R|^2 + 1.04\text{Re}[(1+C_V^L)C_T^*] + 0.75|C_T|^2\}, \quad (16)$$

$$\mathcal{R}(D^*) \simeq \mathcal{R}_{\rm SM}(D^*)\{|1+C_V^L|^2 + 0.13\text{Re}[(1+C_V^L)(C_S^{R*}-C_S^{L*})] + 0.05|C_S^R-C_S^L|^2 - 5.0\text{Re}[(1+C_V^L)C_T^*] + 16.27|C_T|^2\}, \quad (17)$$

$$P_\tau(D) \simeq \left(\frac{\mathcal{R}(D)}{\mathcal{R}_{\rm SM}(D)}\right)^{-1}\{0.32|1+C_V^L|^2 + 1.54\text{Re}[(1+C_V^L)(C_S^{L*}+C_S^{R*})] + 1.09|C_S^L+C_S^R|^2 - 0.35\text{Re}[(1+C_V^L)C_T^*] + 0.05|C_T|^2\}, \quad (18)$$

$$P_\tau(D^*) \simeq \left(\frac{\mathcal{R}(D^*)}{\mathcal{R}_{\rm SM}(D^*)}\right)^{-1}\{-0.49|1+C_V^L|^2 + 0.13\text{Re}[(1+C_V^L)(C_S^{R*}-C_S^{L*})] + 0.05|C_S^R-C_S^L|^2 + 1.67\text{Re}[(1+C_V^L)C_T^*] + 0.93|C_T|^2\}, \quad (19)$$

$$F_L(D^*) \simeq \left(\frac{\mathcal{R}(D^*)}{\mathcal{R}_{\rm SM}(D^*)}\right)^{-1}\{0.46|1+C_V^L|^2 + 0.13\text{Re}[(1+C_V^L)(C_S^{R*}-C_S^{L*})] + 0.05|C_S^R-C_S^L|^2 - 1.98\text{Re}[(1+C_V^L)C_T^*] + 3.2|C_T|^2\}, \quad (20)$$

$$\mathcal{R}(\Lambda_c) \simeq \mathcal{R}_{\rm SM}(\Lambda_c)\{|1+C_V^L|^2 + 0.34\text{Re}[(1+C_V^L)C_S^{L*}] + 0.50\text{Re}[(1+C_V^L)C_S^{R*}] + 0.53\text{Re}[C_S^L C_S^{R*}] + 0.33(|C_S^L|^2+|C_S^R|^2) - 3.10\text{Re}[(1+C_V^L)C_T^*] + 10.44|C_T|^2\}, \quad (21)$$

$$\text{BR}(B_c \to \tau\nu) \simeq 0.02\left(\frac{f_{B_c}}{0.43\ \text{GeV}}\right)^2 |1+C_V^L+4.3(C_S^R-C_S^L)|^2, \quad (22)$$

in terms of the Wilson coefficients defined at the low scale $\mu = m_b$.

The numerical coefficients correspond to the central values of the form factors. Concerning our choice of the form factors, we use the average of Ref. [81] (obtained from two lattice QCD evaluations from Refs. [24,25]) for the vector and scalar form factors entering $B \to D$ transitions. In the case of $B \to D^*$ we adopt the fit results from Ref. [17] for V, A_1, A_2, while for A_0 we employ the result from Ref. [19] using A_1 from Ref. [17] for the normalization. The tensor form factors for

both decay processes are taken from Ref. [19]. We take the value for the B_c meson decay constant, $f_{B_c} = 0.427$ GeV, from Ref. [82], neglecting the small uncertainty. Finally, the complete set of the baryonic form factors for $\Lambda_b \to \Lambda_c \tau\nu$ has recently been provided in Refs. [32,83]; see also Ref. [84].

IV. ANALYSIS OF DIFFERENT NP SCENARIOS

In our statistical analysis we follow the same approach as outlined in Ref. [85], with a further caveat regarding the $\mathrm{BR}(B_c \to \tau\nu)$ constraint (to be discussed below). We build the χ^2 function as

$$\chi^2(C_k) = \sum_{ij}^{N_{\rm obs}} [\mathcal{O}_i^{\rm exp} - \mathcal{O}_i^{\rm th}(C_k)] \mathcal{C}_{ij}^{-1} [\mathcal{O}_j^{\rm exp} - \mathcal{O}_j^{\rm th}(C_k)], \quad (23)$$

where $\mathcal{O}_i^{\rm exp(th)}$ are the measured (predicted) observables and C_k are the Wilson coefficients of the effective Hamiltonian in Eq. (11). In the covariance matrix $\mathcal{C}$, the correlation of $\mathcal{R}(D)$ and $\mathcal{R}(D^*)$ [17] is taken into account. For $F_L(D^*)$ and $P_\tau(D^*)$ we add the statistical and systematic errors in quadrature.

The best-fit point is obtained by minimizing the χ^2 function in the region of parameter space that is compatible with the $\mathrm{BR}(B_c \to \tau\nu)$ constraint. In other words, this constraint is imposed as a hard cut on the parameter space. For this reason, in the scenarios in which a best-fit point is compatible with the $\mathrm{BR}(B_c \to \tau\nu) < 60\%$ constraint, but predicts $10\% < \mathrm{BR}(B_c \to \tau\nu) < 60\%$, imposing the 10% constraint moves the best-fit point to the boundary of the new allowed region in parameter space.

We quantify the goodness-of-fit as a p-value expressing the probability that the remaining differences between theory and experiment are due to statistical fluctuations. This probability corresponds to the one for a χ^2-distributed random variable (having central values in the values predicted at the best-fit point) to reach a higher value than the one obtained from the data, assuming as number of degrees of freedom the difference between the number of observables included in the fit and the number of free parameters fitted. Namely,

$$p\text{-value} = 1 - \mathrm{CDF}_{N_{\rm obs} - N_{\rm par}}(\chi^2_{\rm min}), \quad (24)$$

where CDF_n stands for the cumulative distribution function of a χ^2-distributed random variable with n degrees of freedom, $N_{\rm obs} = 4$ is the number of observables included in the fit, $N_{\rm par}$ is the number of fitted parameters (i.e., $N_{\rm par}^{\rm 1D} = 1$, $N_{\rm par}^{\rm 2D} = 2$) and $\chi^2_{\rm min}$ is the value of the χ^2 at the best-fit point.

For the SM ($N_{\rm par} = 0$) the p-value is

$$p\text{-value}_{\rm SM} \sim 7 \times 10^{-5}, \quad (25)$$

which corresponds to a deviation of data at the 4σ level.

For each scenario, we perform a likelihood ratio test between the best-fit point and a generic point x in parameter space under the assumption that the variables are normally distributed. This test quantifies how much the best-fit point is favored over the other points in the parameter space. In other words, the s-sigma intervals in the 1D and 2D scenarios to be studied correspond to the points x_s in the parameter space such that

$$x_s : \; s(x_s) = \sqrt{\mathrm{CDF}_1^{-1}(\mathrm{CDF}_{N_{\rm par}}(\chi^2(x_s) - \chi^2_{\rm min}))}, \quad (26)$$

where $N_{\rm par} = 1,\ 2$ again stands for the number of fitted parameters. The likelihood ratio test between the

TABLE I. Fit results for the 1D hypotheses (hyp.) defined in Sec. IV A including all available data. The best-fit points and ranges for the Wilson coefficients are quoted for $\mu = 1$ TeV. Note that these results are independent of the choice of the three different limits on $\mathrm{BR}(B_c \to \tau\nu)$. The single exception is the C_S^R scenario, for which the 10% limit leads to a slightly worse fit than the other two. The last six columns show the predictions for the corresponding observable at the best-fit point. For the quantities already measured we list the discrepancy [see Eq. (27)] between the predicted and the experimental value [e.g. for C_S^L the predicted value of $\mathcal{R}(D^*) = 0.247$ at the best-fit point is 4.0σ below the measured value]. Note that the predicted observables are at the same time included in the fit.

1D hyp.	Best fit	1σ range	2σ range	p-value (%)	$\mathrm{Pull}_{\rm SM}$	$\mathcal{R}(D)$	$\mathcal{R}(D^*)$	$F_L(D^*)$	$P_\tau(D^*)$	$P_\tau(D)$	$\mathcal{R}(\Lambda_c)$
C_V^L	0.11	[0.09, 0.13]	[0.06, 0.15]	35	4.6	0.371 -0.8σ	0.312 $+0.4\sigma$	0.46 -1.6σ	−0.49 -0.2σ	0.32	0.40
$C_S^R\vert_{10\%}$	0.15	[0.13, 0.15]	[0.08, 0.15]	1.7	3.8	0.440 $+0.7\sigma$	0.263 -2.8σ	0.48 -1.4σ	−0.44 -0.1σ	0.53	0.38
$C_S^R\vert_{30\%,60\%}$	0.16	[0.13, 0.20]	[0.08, 0.23]	1.8	3.8	0.460 $+1.2\sigma$	0.265 -2.8σ	0.48 -1.3σ	−0.43 -0.1σ	0.55	0.39
C_S^L	0.12	[0.07, 0.16]	[0.01, 0.20]	0.02	2.2	0.412 $+0.1\sigma$	0.247 -4.0σ	0.45 -1.8σ	−0.53 -0.3σ	0.50	0.36
$C_S^L = 4C_T$	−0.07	[−0.12, −0.03]	[−0.15, 0.02]	0.01	1.6	0.242 -3.6σ	0.280 -1.7σ	0.46 -1.6σ	−0.45 -0.1σ	0.18	0.34

TABLE II. Results of the fit for the Wilson coefficients (given at the matching scale of 1 TeV) for the 2D hypotheses (hyp.) defined in Sec. IV B including all available data with $\mathrm{BR}(B_c \to \tau\nu) < 60\%$, $\mathrm{BR}(B_c \to \tau\nu) < 30\%$ and $\mathrm{BR}(B_c \to \tau\nu) < 10\%$, respectively. In case there is no label for the constraint on $\mathrm{BR}(B_c \to \tau\nu)$ used, the fit is valid for all three benchmark scenarios.

2D hyp.	Best fit	p-value (%)	$\mathrm{Pull}_{\mathrm{SM}}$	$\mathcal{R}(D)$	$\mathcal{R}(D^*)$	$F_L(D^*)$	$P_\tau(D^*)$	$P_\tau(D)$	$\mathcal{R}(\Lambda_c)$
$(C_V^L, C_S^L = -4C_T)$	(0.08, 0.05)	22.0	4.2	0.394 -0.3σ	0.308 $+0.2\sigma$	0.45 -1.7σ	−0.50 -0.2σ	0.40	0.41
$(C_S^R, C_S^L)\|_{60\%}$	(−0.19, −0.74) (0.34, −0.22)	68.5	4.5	0.412 $+0.1\sigma$	0.299 -0.5σ	0.54 -0.7σ	−0.27 $+0.2\sigma$	0.50	0.40
$(C_S^R, C_S^L)\|_{30\%}$	(−0.30, −0.64) (0.24, −0.11)	11.8	4.1	0.423 $+0.4\sigma$	0.280 -1.8σ	0.51 -1.0σ	−0.35 0.0σ	0.51	0.39
$(C_S^R, C_S^L)\|_{10\%}$	(0.14, 0.00) (−0.40, −0.55)	0.6	3.4	0.433 $+0.6\sigma$	0.263 -2.9σ	0.48 -1.4σ	−0.44 -0.1σ	0.53	0.38
(C_V^L, C_S^R)	(0.09, 0.06)	30.8	4.3	0.413 $+0.1\sigma$	0.305 -0.1σ	0.47 -1.5σ	−0.47 -0.2σ	0.41	0.42
$(\mathrm{Re}[C_S^L = 4C_T], \mathrm{Im}[C_S^L = 4C_T])\|_{60,30\%}$	$(-0.06, \pm 0.40)$	22.0	4.2	0.404 -0.1σ	0.306 0.0σ	0.45 -1.7σ	−0.39 0.0σ	0.50	0.41
$(\mathrm{Re}[C_S^L = 4C_T], \mathrm{Im}[C_S^L = 4C_T])\|_{10\%}$	$(-0.02, \pm 0.24)$	0.3	3.2	0.339 -1.5σ	0.274 -2.2σ	0.46 -1.7σ	−0.45 -0.1σ	0.40	0.36

best-fit point and the SM, i.e., the SM-pull, is defined as the p-value corresponding to $\chi^2_{\mathrm{SM}} - \chi^2_{\mathrm{min}}$, with $\chi^2_{\mathrm{SM}} = \chi^2(0)$, and is then expressed in terms of standard deviations (σ).

The discrepancies of the measured observables in Tables I and II are defined as the difference between the predicted value at the best-fit point and data, expressed as multiples of the experimental error ($\sigma^{\mathcal{O}_i^{\mathrm{exp}}}$), i.e.,

$$\mathrm{d}_{\mathcal{O}_i} = \frac{\mathcal{O}_i^{\mathrm{NP}} - \mathcal{O}_i^{\mathrm{exp}}}{\sigma^{\mathcal{O}_i^{\mathrm{exp}}}}. \tag{27}$$

A. One-dimensional scenarios

In a first step, we consider one-dimensional scenarios (with real Wilson coefficients) which can be generated by a single new particle added to the SM:

(i) C_V^L: This setup arises in models with vector leptoquarks (LQs) like the $\mathrm{SU}(2)_L$-singlet vector LQ of the Pati-Salam model (U_1) [86–106], the scalar $\mathrm{SU}(2)_L$-triplet and/or scalar $\mathrm{SU}(2)_L$-singlet LQ [40,47,107–113] (with left-handed couplings only) or in models with left-handed W' bosons [114–117].

(ii) C_S^R: This operator is generated in models with extra charged scalars. In particular it is the dominant operator in 2HDMs of type II in the large $\tan\beta$ region (see, e.g., Refs. [118,119] for an early account) and can be generated with the $\mathrm{SU}(2)_L$-doublet vector LQ (V_2) [120,121].

(iii) C_S^L: This setup is again motivated by models with extra charged scalars. However, here a generic flavor structure is needed to make O_S^L the dominant operator [122–131].

(iv) $C_S^L = 4C_T$: $C_S^L = 4C_T$ at the NP scale is generated by the scalar $\mathrm{SU}(2)_L$-doublet S_2 (also called R_2) LQ [132,133]. However, QCD renormalization-group (RG) effects from the NP scale down to the m_b scale change this relation. Furthermore, electroweak RG effects mix the left-handed scalar and tensor operators above the electroweak symmetry breaking scale [71,134]. Taking into account these effects for NP of $\mathcal{O}(\mathrm{TeV})$ we use $C_S^L \simeq 8.1 C_T$ at the scale $\mu = m_b$ [71].

In Fig. 1, we show the $\Delta\chi^2(C_i) \equiv \chi^2(C_i) - \chi^2_{\mathrm{SM}}$ (i.e., the difference compared to the χ^2 in the SM as a function of the Wilson coefficients) for these four cases. The dashed lines correspond to the situation before the $F_L(D^*)$ measurement

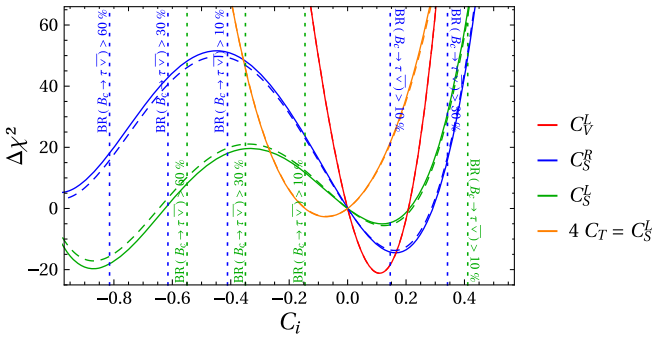

FIG. 1. $\Delta\chi^2$ for the four one-dimensional scenarios in which only a single real Wilson coefficient (at the TeV scale) receives a NP contribution. The dashed lines show the situation before the $F_L(D^*)$ measurement, while the solid lines include the latter. The dotted vertical lines correspond to the limit on $C_S^{L,R}$ from $\mathrm{BR}(B_c \to \tau\nu)$ assuming a maximal value of 10%, 30% and 60% (i.e., the outer side of these lines is excluded by the corresponding constraint). Thus, only a 10% limit on $\mathrm{BR}(B_c \to \tau\nu)$ can exclude the best-fit point for C_S^R while for C_S^L this point is always excluded and only positive values can provide a good fit to data.

and the solid lines depict the situation once $F_L(D^*)$ is included. One can see from the plot that while the vector operator still gives the best fit to the data, $F_L(D^*)$ slightly improves the agreement of the C_S^R scenario with data in the vicinity of the best-fit point. The dotted vertical lines delimit the area allowed by different bounds on $\mathrm{BR}(B_c \to \tau\nu)$, which is only relevant for the C_S^L and C_S^R scenarios. One observes that even for the conservative limit $\mathrm{BR}(B_c \to \tau\nu) \leq 60\%$ negative solutions for C_S^L and C_S^R are disfavored with respect to the SM point.

Table I summarizes the results for the four 1D scenarios. Here we give the best-fit point, the corresponding 1σ and 2σ ranges around this point, as well as the p-value (characterizing the goodness of the fit) and the pull with respect to the SM. The last six columns show the predictions for the observables under consideration at the best-fit point. In addition, the discrepancy [defined in Eq. (27)] between the predicted value for the observables and the current measurement is given for those observables for which a measurement is available.

Let us illustrate this with the C_S^L scenario as an example. Here, if the best-fit point $C_S^L = 0.12$ is realized in nature, the probability that statistical fluctuations would account for the remaining discrepancy between theory and data is 0.02%; i.e., the scenario describes the data poorly. This can be attributed to the fact that the predicted values of $\mathcal{R}(D^*)$ and $F_L(D^*)$ are below their measured values by 4.0 and 1.8 standard deviations, respectively. $\mathrm{BR}(B_c \to \tau\nu)$ is important for this scenario because it excludes the otherwise favored value $C_S^L \sim -0.9$, as can be seen in Fig. 1, independent of which of the three limits we choose. The value of the SM pull, $\mathrm{pull}_{\mathrm{SM}} = 2.2\sigma$, shows that $C_S^L = 0.12$ describes the data only moderately better than $C_S^L = 0$.

The hypothesis of NP entering through C_V^L has a favorable p-value of 35% and the $C_S^L = 4C_T$ scenario gives the worst fit. As a caveat, we recall that we have restricted ourselves to real values of the coefficients. Therefore, if complex values for $C_S^L = 4C_T$ are permitted the situation will change. However, we do not consider complex values for the Wilson coefficients in the other three scenarios. For C_V^L this would not change the predictions and for C_S^L and C_S^R complex values are constrained by $\mathrm{BR}(B_c \to \tau\nu)$.

Note that the results are quite independent of the bound used for the contribution to $\mathrm{BR}(B_c \to \tau\nu)$. The significance of the four one-dimensional scenarios does not change depending on whether one uses the conservative bound of 60% or the most commonly used one of 30% for $\mathrm{BR}(B_c \to \tau\nu)$. Furthermore, only the C_S^R scenario is slightly affected once the hypothetical future limit of 10% is used; the p-value changes slightly from 1.8% to 1.7%. Also note that in the C_V^L-scenario polarization observables $F_L(D^*), P_\tau(D^*)$ and $P_\tau(D)$ are unchanged with respect to the SM. Therefore, a significant deviation in these observables would automatically disfavor (or potentially exclude) this scenario.

B. Two-dimensional scenarios

Let us now consider several two-dimensional hypotheses. Again, we consider only scenarios which can be generated by adding a single new field to the SM particle content.

(i) $(C_V^L, C_S^L = -4C_T)$: This setup is obtained in models with an $\mathrm{SU}(2)_L$-singlet scalar LQ (S_1). Here the relation $C_S^L = -4C_T$ is again assumed at the NP scale. Through the RG running mentioned above, starting from an $\mathcal{O}(\mathrm{TeV})$ matching scale, the relation becomes $C_S^L \simeq -8.5C_T$ at the low scale [71].

(ii) (C_S^R, C_S^L): As for the 1D cases, this scenario is motivated by charged Higgs exchange.

(iii) (C_V^L, C_S^R): This setup is generated by models with vector LQs like the $\mathrm{SU}(2)_L$-singlet LQ U_1.

(iv) $(\mathrm{Re}[C_S^L = 4C_T], \mathrm{Im}[C_S^L = 4C_T])$: At the high scale, this relation is generated by the scalar $\mathrm{SU}(2)_L$-doublet LQ S_2. As in the 1D case, RG effects modify this relation to $C_S^L \simeq 8.1C_T$ at the scale $\mu = m_b$. Here we consider complex couplings because, as seen in the previous subsection, real parameters do not give a good fit to the data. On the other hand, as shown in Ref. [133], complex Wilson coefficients are able to reproduce the $\mathcal{R}(D^{(*)})$ data.

The results of these fits are given in Table II, for a limit on $\mathrm{BR}(B_c \to \tau\nu)$ of 60%, 30% and 10%, respectively. We treat again the $\mathrm{BR}(B_c \to \tau\nu)$ constraint as a hard limit. Note that the $\mathrm{BR}(B_c \to \tau\nu)$ constraint has no impact on the best-fit points of the $(C_V^L, C_S^L = -4C_T)$ and (C_V^L, C_S^R) scenarios. For the $(\mathrm{Re}[C_S^L = 4C_T], \mathrm{Im}[C_S^L = 4C_T])$ scenario, only the hypothetical future bound of 10% significantly reduces the goodness of the fit (from 22% to 0.3%). The impact on the (C_S^R, C_S^L) scenario is very significant: while for the most conservative limit of 60% this scenario gives the best fit among all the scenarios considered, the agreement with data is only moderate for the 30% limit and even very bad for the 10% one. Note that the tension arises only in $\mathcal{R}(D^*)$ which is governed by the same coupling $C_S^R - C_S^L$ as $\mathrm{BR}(B_c \to \tau\nu)$.

The content of Table II translates to the plots shown in Fig. 2. Here, one can see that if the overall best-fit point is excluded by the $\mathrm{BR}(B_c \to \tau\nu)$ limit, the point with the minimum χ^2 compatible with this bound is taken instead. Thus, the new best-fit point lies on the boundary of the region excluded by $\mathrm{BR}(B_c \to \tau\nu)$, and it is surrounded by the corresponding confidence region. Therefore, different limits for $\mathrm{BR}(B_c \to \tau\nu)$ lead to different preferred regions, and the best-fit points are also distinct concerning the overall goodness (the p-value) of the fit. In the last six columns of Table II we give again the predictions of the

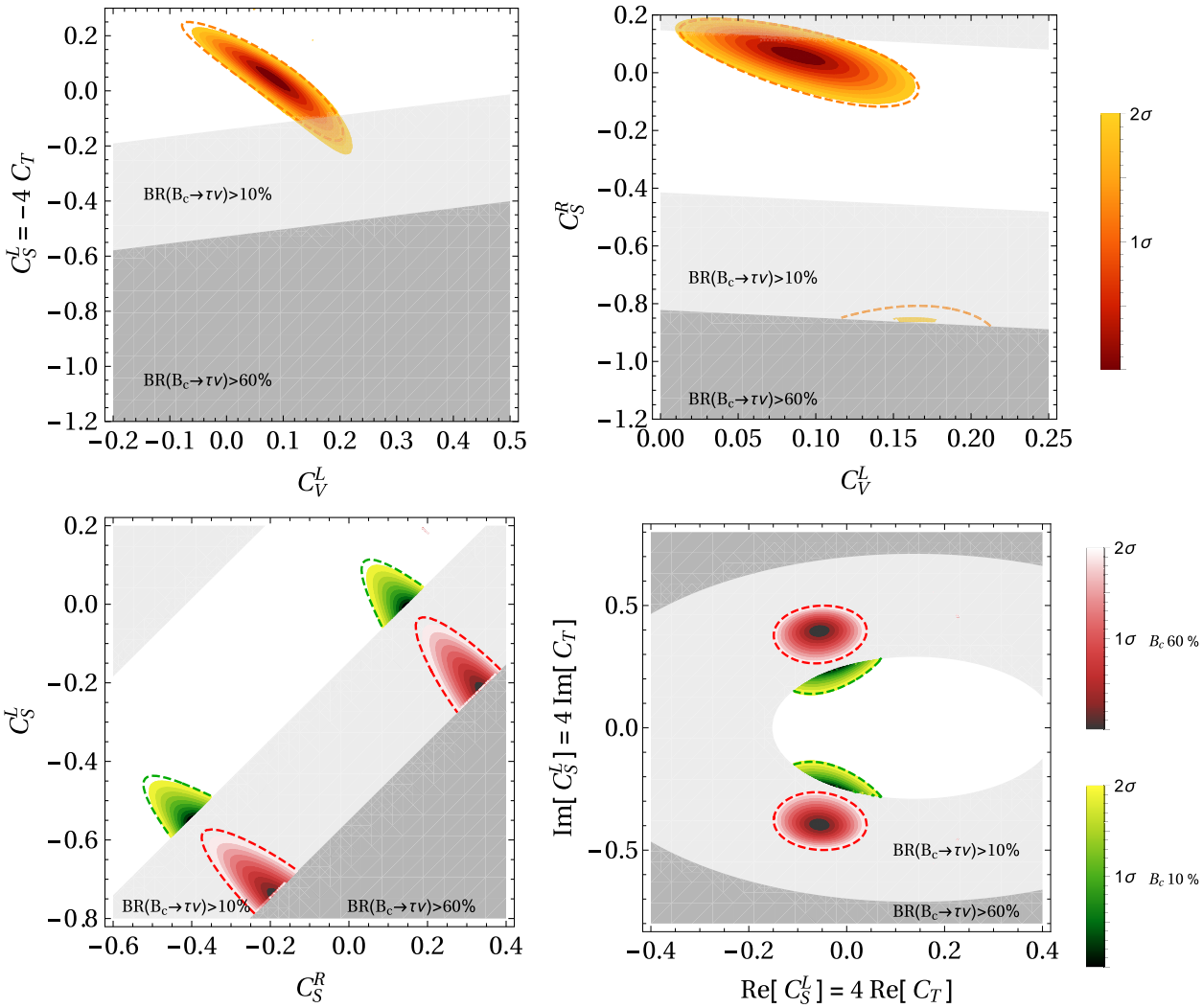

FIG. 2. Results of the fits in the two-dimensional NP scenarios, with Wilson coefficients given at the matching scale of 1 TeV. The p-values of the best fit are given in Table II. The dashed ellipses show the situation before the $F_L(D^*)$ measurement at the 2σ level, while the colored regions include $F_L(D^*)$. We impose either a 60% or a 10% limit on $\mathrm{BR}(B_c \to \tau\nu)$. The scenarios shown in the upper plots (orange color coding) are not affected by either of these constraints. In the scenarios shown in the lower plots the best-fit points and the corresponding σ-regions move when we consider a 10% (green color coding) constraint instead of the 60% one.

observables and their discrepancy [defined in Eq. (27)] with the experimental value.

V. CORRELATIONS BETWEEN OBSERVABLES

Let us now assess the future discriminatory power of the various $b \to c\tau\nu$ observables and evaluate the correlations among the observables within our two-dimensional scenarios of Sec. IV B.

Let us start with the correlations among $\mathcal{R}(D^{(*)})$ and $\mathcal{R}(\Lambda_c)$ as shown in Fig. 3. The colored regions in the $\mathcal{R}(D^{(*)})$–$\mathcal{R}(\Lambda_c)$ plane are allowed at the 1σ level as obtained by the fit (see Fig. 2). In addition, the different bounds from $\mathrm{BR}(B_c \to \tau\nu)$ are shown. As seen in the previous section, this bound is irrelevant for the $(C_V^L, C_S^L = -4C_T)$ and (C_V^L, C_S^R) scenarios and also does not affect the complex $(C_S^L = +4C_T)$ scenario, unless the hypothetical future bound of 10% is used. However, for the (C_S^R, C_S^L) scenario it puts a stringent upper bound on $\mathcal{R}(\Lambda_c)$ depending on $\mathcal{R}(D)$.

Interestingly, we find very similar patterns for $\mathcal{R}(\Lambda_c)$ in all scenarios and always predict an enhancement of $\mathcal{R}(\Lambda_c)$ over its SM value. We trace this behavior back to a *sum rule*, which can be derived from the expressions in Eqs. (16), (17) and (22):

$$\frac{\mathcal{R}(\Lambda_c)}{\mathcal{R}_{\mathrm{SM}}(\Lambda_c)} = 0.262\frac{\mathcal{R}(D)}{\mathcal{R}_{\mathrm{SM}}(D)} + 0.738\frac{\mathcal{R}(D^*)}{\mathcal{R}^{\mathrm{SM}}(D^*)} + x, \quad (28)$$

where the small remainder x is well approximated by

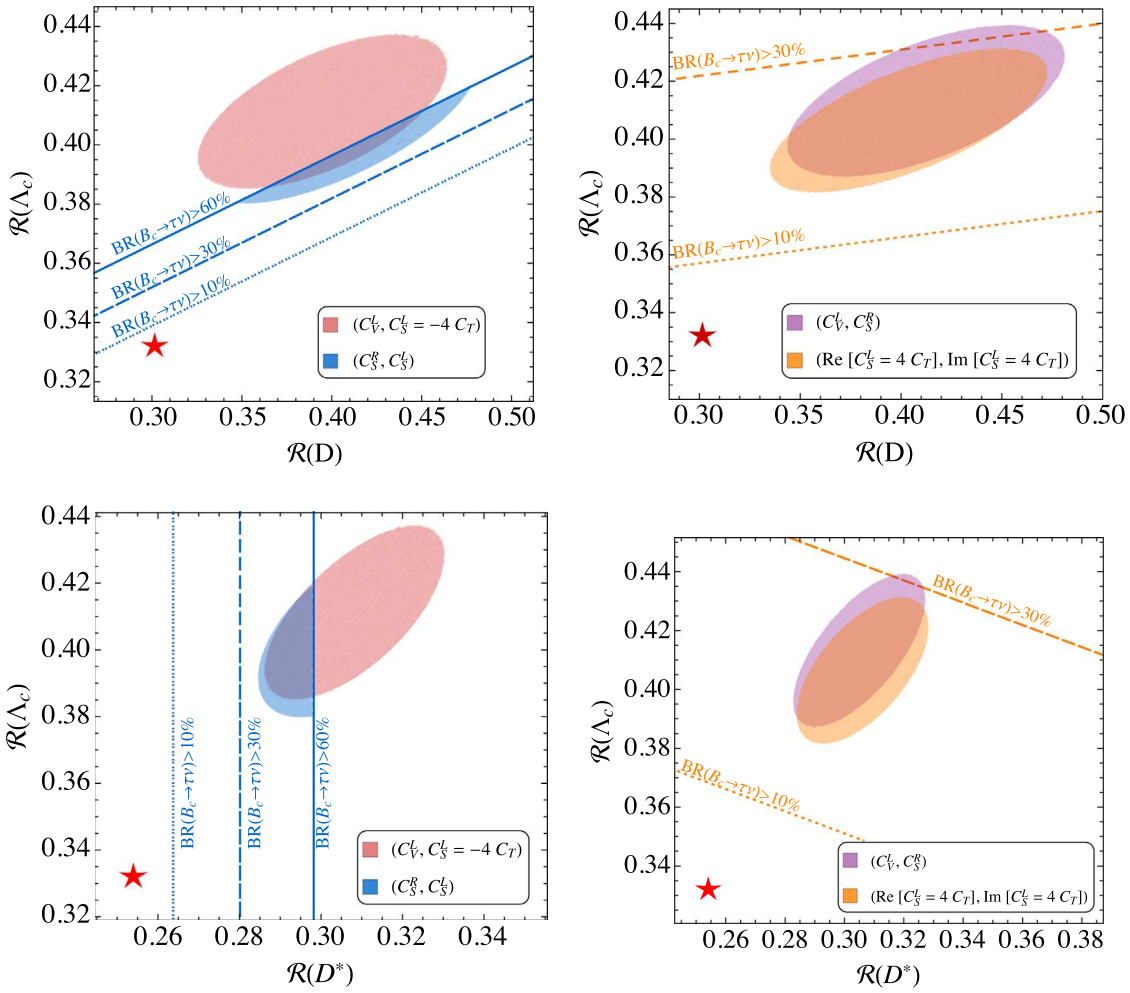

FIG. 3. Preferred 1σ regions in the four two-dimensional scenarios in the $\mathcal{R}(D^{(*)})$–$\mathcal{R}(\Lambda_c)$ plane for $\mathrm{BR}(B_c \to \tau\nu) < 60\%$. The regions of the plot in the left panel correspond to the scenarios $(C_V^L, C_S^L = -4C_T)$ (red) and (C_S^R, C_S^L) (blue), while the plots on the right side correspond to (C_V^L, C_S^R) (purple) and $(C_S^L = 4C_T)$ (orange). The solid, dashed and dotted lines refer to a limit on $\mathrm{BR}(B_c \to \tau\nu)$ of 60%, 30% and 10%, respectively. The stars represent the SM predictions.

$$x \simeq -\mathrm{Re}[(1 + C_V^L)(0.32C_T^* + 0.03C_S^{L*})] + 1.76|C_T|^2 - 0.0075|C_S^L|^2 - 0.033\mathrm{Re}(C_S^L C_S^{R*}), \quad (29)$$

with all coefficients evaluated at $\mu = m_b$. The consequences of this sum rule are best visible in Fig. 6, where the $\mathcal{R}(\Lambda_c)$ contours are essentially the same straight lines. Evolving the best-fit points of Table II to $\mu = m_b$ with Eq. (13) (and using the exact formula for x) we find $x = 6 \cdot 10^{-4}$, $x = 1 \cdot 10^{-2}$, $x = -1 \cdot 10^{-4}$, and $x = 5 \cdot 10^{-3}$ for the four scenarios. Even beyond the considered scenarios and permitting more than two coefficients to be nonzero one finds $|x| < 0.05$ if the coefficients are chosen to explain $\mathcal{R}(D)$ and $\mathcal{R}(D^*)$. So $\mathcal{R}(\Lambda_c)$ must be enhanced over the SM value if $\mathcal{R}(D)$ and $\mathcal{R}(D^*)$ are. The existence of the sum rule in Eq. (28), which holds in *any* model of new physics, implies that a future measurement of $\mathcal{R}(\Lambda_c)$ will serve as a check of the measurements of $\mathcal{R}(D)$ and $\mathcal{R}(D^*)$ and of the form-factor calculations. For all of our four two-dimensional scenarios we predict

$$\mathcal{R}(\Lambda_c) = \mathcal{R}_{\mathrm{SM}}(\Lambda_c)(1.24 \pm 0.06) = 0.41 \pm 0.02 \pm 0.01, \quad (30)$$

where the first error stems from the experimental errors in $\mathcal{R}(D^{(*)})$ in Eq. (2) and the second error in Eq. (30) reflects the present uncertainties of the form-factor ratios.

Figure 4 reveals interesting correlations between polarization observables, including the yet unmeasured tau polarization in the $B \to D\tau\nu$ decay mode. These correlations provide a strong tool to discriminate between different NP scenarios, especially in the cases in which the predicted regions shrink effectively to a line (i.e., exhibit direct correlations). In the case of the correlation between $P_\tau(D^*)$

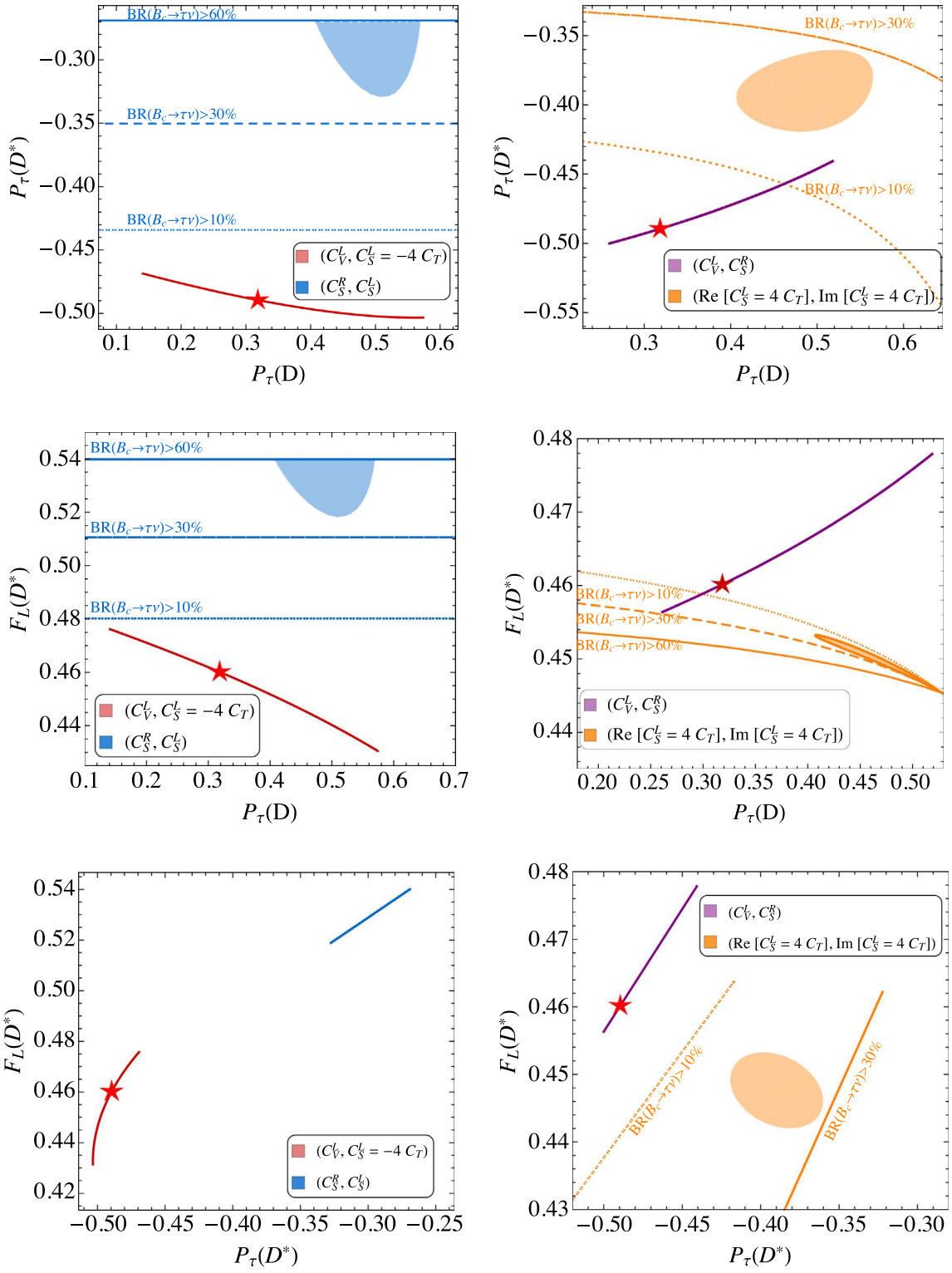

FIG. 4. Pairwise correlations between the observables $P_\tau(D), P_\tau(D^*)$ and $F_L(D^*)$. The predicted 1σ regions in the four two-dimensional scenarios [assuming $\mathrm{BR}(B_c \to \tau\nu) < 60\%$] are shown. The color coding is the same as in Fig. 3. Note that in some cases the preferred regions shrink to lines, revealing the tight correlations between two observables in a given scenario. However, it is important to keep in mind that these correlations are obtained in the limit of vanishing form-factor uncertainties. Therefore, they represent the ideal correlations which can only in principle be obtained in a given scenario.

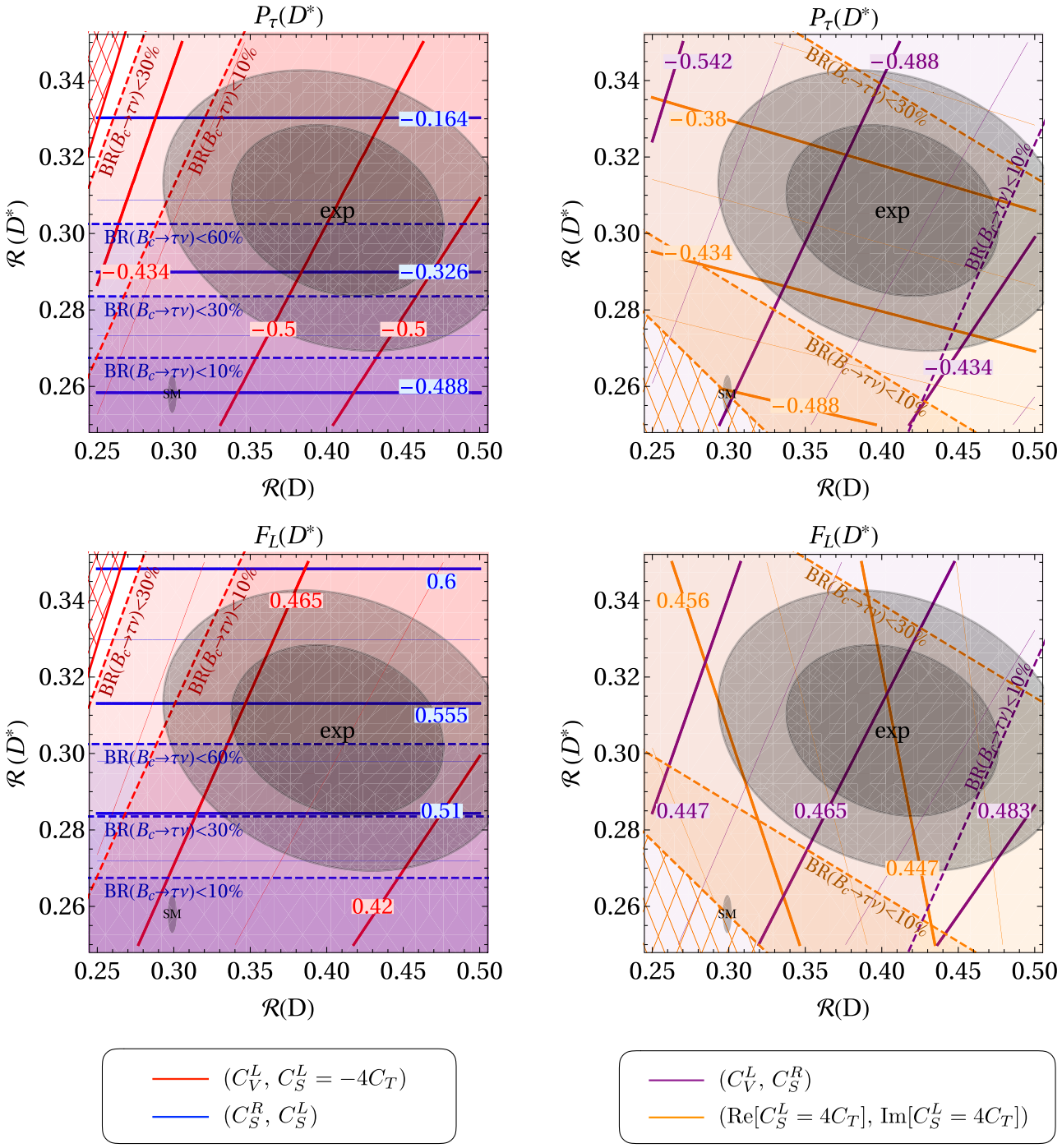

FIG. 5. Contour lines of the τ polarization and the longitudinal D^* polarization for the two-dimensional scenarios in the $\mathcal{R}(D)$–$\mathcal{R}(D^*)$ plane. The colored regions (bounded by dashed lines) are allowed by the 10%, 30% and 60% limits on $\mathrm{BR}(B_c \to \tau\nu)$, where any area that would fill the entire plot is not shown for convenience. The contours show the predicted values for the various observables (for vanishing form-factor uncertainties). The thin lines carrying no labels depict the arithmetic means of the neighboring thick lines. The gray regions are currently preferred by data at the 1 and 2σ levels. The colored, hatched regions are excluded in the specific scenarios. Interestingly, the different scenarios exhibit distinct correlations among the observables, manifesting themselves in the different slopes of the contours and the different values associated with them.

and $F_L(D^*)$ considered within the (C_S^R, C_S^L) scenario (plot in the third row on the left) this follows trivially since both observables are affected by the pseudoscalar combination $C_S^R - C_S^L$ only. The tight correlations in the other cases are, on the other hand, a result of the polarization observables being insensitive to the value of C_V^L. However, it is very important to keep in mind that these correlations are obtained for vanishing uncertainties of the form factors.

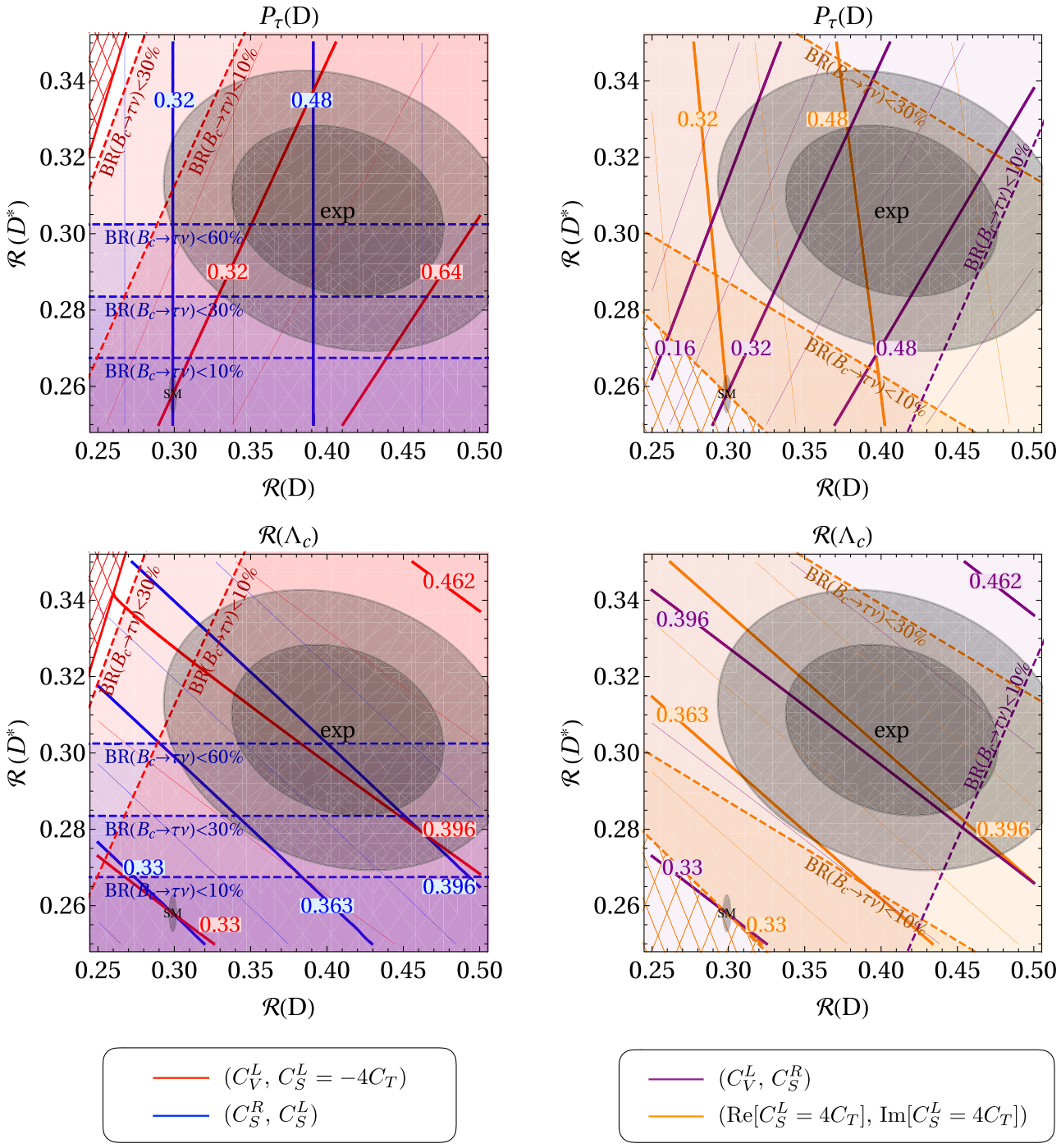

FIG. 6. Contour lines of $P_\tau(D)$ and $\mathcal{R}(\Lambda_c)$ for the two-dimensional scenarios in the $\mathcal{R}(D)$–$\mathcal{R}(D^*)$ plane. The colored regions (bounded by dashed lines) are allowed by the 10%, 30% and 60% limits on $\mathrm{BR}(B_c \to \tau\nu)$, where any area that would fill the entire plot is not shown for convenience. The contours show the predicted value for the various observables (neglecting the errors of the form factors). The thin lines carrying no labels depict the arithmetic means of the neighboring thick lines. The gray regions are currently preferred by data at the 1 and 2σ level and the colored, hatched regions are excluded in the specific scenarios. Interestingly, the different scenarios display distinct correlations among the observables [except for $R(\Lambda_c)$], manifesting themselves in the different slopes of the contours and the different values associated with them.

Therefore, they represent the correlations which can only in principle be obtained in a given scenario. Therefore, for exploiting such correlations future improvements on the theory predictions for form factors are imperative.

Let us now turn to future predictions and impact of the polarization observables. Here, we consider again the four two-dimensional scenarios of Sec. IV B. However, this time we do not use $F_L(D^*)$, the tau polarizations as inputs for

the fit, but rather predict them as a function of $\mathcal{R}(D)$ and $\mathcal{R}(D^*)$. This is shown in Figs. 5 and 6. While the current experimental data for $P_\tau(D^*)$ do not significantly discriminate between the different scenarios, the preliminary $F_L(D^*)$ measurement shows a tension in the scenarios $(C_V^L, C_S^L = -4C_T)$ and complex $C_S^L = 4C_T$. Furthermore, future measurements of $F_L(D^*)$ can be used to differentiate between different scenarios. This can be seen from the different slopes of the contour lines and the quite different values associated to them comparing the four scenarios.

VI. CONCLUSIONS

Tauonic B meson decays are excellent probes of physics beyond the SM (complementary to the direct searches at the LHC) since they are sensitive to lepton flavor universality violation in the tau sector, e.g., to Higgs bosons, W' bosons and leptoquarks. In order to distinguish different models, it is very important to be able to assess the presence of scalar and/or tensor operators: while Higgs bosons only generate scalar operators, LQs generate vector operators and possibly also scalar or tensor ones, while W' bosons only give rise to vector operators. Thus, on the one hand, establishing the presence of scalar operators would rule out (pure) W' explanations while the presence of vector operators would exclude (pure) charged Higgs models. On the other hand, the combination of vector operators with scalar and/or tensor ones would be a strong indication for LQs.

In this respect, the current Belle measurement of $F_L(D^*)$ is very important and the limit on the NP contribution to $\mathrm{BR}(B_c \to \tau\nu)$ is crucial to establish or disprove scalar contributions. Together with the measurements of the ratios $\mathcal{R}(D)$, $\mathcal{R}(D^*)$, $\mathcal{R}(J/\Psi)$, these observables can be used in the future to identify the Lorentz structure of NP.

In this article we studied four one-dimensional scenarios (all with real Wilson coefficients) C_V^L, C_S^R, C_S^L, and $C_S^L = 4C_T$ and the four two-dimensional scenarios $(C_V^L, C_S^L = -4C_T)$; (C_S^R, C_S^L); (C_V^L, C_S^R); and $(\mathrm{Re}[C_S^L = 4C_T], \mathrm{Im}[C_S^L = 4C_T])$. All these scenarios have in common that they can be generated by the exchange of a single new particle. The fit results are shown in Tables I and II.

For these scenarios we critically reconsidered the limits on the NP contribution to the decay $B_c \to \tau\nu$. Here we stress that the 10% limit [77] on $\mathrm{BR}(B_c \to \tau\nu)$ from $Z \to b\bar{b}$ decays at LEP suffers from uncertainties related to the hadronization probability of a b quark into a B_c meson and should not be taken at face value. Furthermore, also the more conservative 30% limit of Ref. [36] is not strict since the error of the theory calculation of the B_c lifetime has not fully been taken into account. Therefore, a conservative limit of 60% seems reasonable. Concerning the one-dimensional scenarios we found that the impact of the choice of the limit on $\mathrm{BR}(B_c \to \tau\nu)$ on the fit is very limited; only the C_S^R scenario (which does not give a good fit to data anyway) is slightly affected if the hypothetical future bound of 10% is chosen while the C_V^L scenario always gives by far the best fit. However, on the two-dimensional scenarios the choice of the $\mathrm{BR}(B_c \to \tau\nu)$ limit has a significant impact. Using the conservative 60% limit the (C_S^R, C_S^L) scenario gives the best fit to data, while when enforcing the 30% limit the agreement with data is significantly worse and for the 10% limit this scenario is even strongly disfavored.

Next we studied the predictions for $\mathcal{R}(\Lambda_c)$ finding a *sum rule* relating this ratio to $\mathcal{R}(D)$ and $\mathcal{R}(D^*)$, independent of any NP scenario up to small corrections. This implies that $\mathcal{R}(\Lambda_c)$ does not provide additional information on the Lorentz structure of NP but provides an important consistency check of the $\mathcal{R}(D)$ and $\mathcal{R}(D^*)$ measurements.

Finally, we considered the correlations among polarization observables and predicted them as functions of $\mathcal{R}(D)$ and $\mathcal{R}(D^*)$. Here we found strong correlations among the polarization observables, depending on the scenario chosen (see Fig. 4). Disregarding the form-factor uncertainties, even direct correlations are found. In the (C_S^R, C_S^L) scenario this is due to the equal dependence of the observables on the Wilson coefficients while in the other cases the correlation is a result of the polarization observables being insensitive to the value of C_V^L. Furthermore, the polarization observables show a unique dependence on $\mathcal{R}(D)$ and $\mathcal{R}(D^*)$ for the different observables (see Figs. 5 and 6).

Therefore, future measurements of polarization observables together with $\mathcal{R}(D)$ and $\mathcal{R}(D^*)$ will be able to determine the Lorentz structure of NP while $\mathcal{R}(\Lambda_c)$ will serve as a consistency check. In this way different models (e.g., W', leptoquark and charged Higgs) can in principle be distinguished. However, for this exciting perspective also improved theory predictions for the form factors and $\mathrm{BR}(B_c \to \tau\nu)$ are crucial.

ACKNOWLEDGMENTS

The work of A. C. is supported by an Ambizione Grant of the Swiss National Science Foundation (Grant No. PZ00P2_154834). M. M. acknowledges the support of the DFG-funded Doctoral School "Karlsruhe School of Elementary and Astroparticle Physics: Science and Technology." The work of S. dB., I. N., and U. N. is supported by BMBF under Grant No. 05H18VKKB1. We thank Syuhei Iguro, Yuji Omura, Ryoutaro Watanabe and Kei Yamamoto for sharing with us their draft of "D^* polarization vs $R_{D^{(*)}}$ anomalies in the leptoquark models" [135] prior to its publication. We acknowledge extensive discussions with Andrew Akeroyd about Ref. [77] and thank Admir Greljo for guiding us through Refs. [136,137].

Note Added.—Recently Ref. [136] appeared which studies the constraints from the high-p_T tails in mono-τ searches on the effective field theory (EFT) operators mediating

$b \to c\tau\nu$ and specific UV completions. The authors have found that the EFT analysis is valid for certain leptoquark models if the leptoquarks are sufficiently heavy, while UV completions with the exchange of a colorless particle in the s-channel require an explicit model-dependent study beyond the EFT framework. In Ref. [136] a few scenarios are found for which already present high-p_T data pose useful constraints on the Wilson coefficients, challenging these scenarios as explanations of the $b \to c\tau\nu$ anomaly, but none of these scenarios is considered in this paper. However, we find that the study of Ref. [136] constrains our two-dimensional scenario with complex $C_S^L = 4C_T$, corresponding to the exchange of a (sufficiently heavy) leptoquark S_2. Inferring the allowed region from Ref. [137], we realize that the best-fit point of the scenarios with $\mathrm{BR}(B_c \to \tau\nu) < 30\%, 60\%$ (see Table II) and a large portion of the corresponding 2σ area (in red) in the lower right plot of Fig. 2 is excluded by the 2σ bound $|C_S^L| \lesssim 0.35$ from high-p_T data. This latter bound qualitatively mimics a stricter bound on $\mathrm{BR}(B_c \to \tau\nu)$, which would also push $|C_S^L| = 4|C_T|$ to a smaller value. Thus if the S_2 scenario is realized in nature, we can expect effects in high-p_T tails in mono-τ searches or eventually even the discovery of the S_2 leptoquark by ATLAS or CMS.

[1] G. Ricciardi, Mod. Phys. Lett. A **32**, 1730005 (2017).
[2] B. Grinstein, Proc. Sci., HQL2016 (**2017**) 061.
[3] F. De Fazio, Proc. Sci., EPS-HEP2017 (**2017**) 210.
[4] U. Nierste, S. Trine, and S. Westhoff, Phys. Rev. D **78**, 015006 (2008).
[5] J. F. Kamenik and F. Mescia, Phys. Rev. D **78**, 014003 (2008).
[6] S. Fajfer, J. F. Kamenik, and I. Nisandzic, Phys. Rev. D **85**, 094025 (2012).
[7] R. Alonso, J. Martin Camalich, and S. Westhoff, Phys. Rev. D **95**, 093006 (2017).
[8] J. P. Lees *et al.* (*BABAR* Collaboration), Phys. Rev. Lett. **109**, 101802 (2012).
[9] J. P. Lees *et al.* (*BABAR* Collaboration), Phys. Rev. D **88**, 072012 (2013).
[10] M. Huschle *et al.* (Belle Collaboration), Phys. Rev. D **92**, 072014 (2015).
[11] Y. Sato *et al.* (Belle Collaboration), Phys. Rev. D **94**, 072007 (2016).
[12] S. Hirose *et al.* (Belle Collaboration), Phys. Rev. Lett. **118**, 211801 (2017).
[13] S. Hirose *et al.* (Belle Collaboration), Phys. Rev. D **97**, 012004 (2018).
[14] R. Aaij *et al.* (LHCb Collaboration), Phys. Rev. Lett. **115**, 111803 (2015); **115**, 159901(E) (2015).
[15] R. Aaij *et al.* (LHCb Collaboration), Phys. Rev. Lett. **120**, 171802 (2018).
[16] R. Aaij *et al.* (LHCb Collaboration), Phys. Rev. D **97**, 072013 (2018).
[17] Y. Amhis *et al.* (HFLAV Collaboration), Eur. Phys. J. C **77**, 895 (2017), updated average of $R(D)$ and $R(D^*)$ for Summer 2018 at https://hflav-eos.web.cern.ch/hflav-eos/semi/summer18/RDRDs.html.
[18] D. Bigi and P. Gambino, Phys. Rev. D **94**, 094008 (2016).
[19] F. U. Bernlochner, Z. Ligeti, M. Papucci, and D. J. Robinson, Phys. Rev. D **95**, 115008 (2017); **97**, 059902(E) (2018).
[20] D. Bigi, P. Gambino, and S. Schacht, J. High Energy Phys. 11 (2017) 061.
[21] S. Jaiswal, S. Nandi, and S. K. Patra, J. High Energy Phys. 12 (2017) 060.
[22] D. Becirevic and N. Kosnik, Acta Phys. Pol. Proc. Suppl. **3**, 207 (2010).
[23] S. de Boer, T. Kitahara, and I. Nisandzic, Phys. Rev. Lett. **120**, 261804 (2018).
[24] J. A. Bailey *et al.* (MILC Collaboration), Phys. Rev. D **92**, 034506 (2015).
[25] H. Na, C. M. Bouchard, G. P. Lepage, C. Monahan, and J. Shigemitsu (HPQCD Collaboration), Phys. Rev. D **92**, 054510 (2015); **93**, 119906(E) (2016).
[26] R. Aaij *et al.* (LHCb Collaboration), Phys. Rev. Lett. **120**, 121801 (2018).
[27] C. W. Murphy and A. Soni, Phys. Rev. D **98**, 094026 (2018).
[28] T. D. Cohen, H. Lamm, and R. F. Lebed, J. High Energy Phys. 09 (2018) 168.
[29] C.-T. Tran, M. A. Ivanov, J. G. Körner, and P. Santorelli, Phys. Rev. D **97**, 054014 (2018).
[30] R. Watanabe, Phys. Lett. B **776**, 5 (2018).
[31] B. Chauhan and B. Kindra, arXiv:1709.09989.
[32] W. Detmold, C. Lehner, and S. Meinel, Phys. Rev. D **92**, 034503 (2015).
[33] K. Adamczyk, *B* to semitauonic decays at Belle/Belle II, in Proceedings of the 10th International Workshop on the CKM Unitarity Triangle, Heidelberg (2018).
[34] A. K. Alok, D. Kumar, S. Kumbhakar, and S. U. Sankar, Phys. Rev. D **95**, 115038 (2017).
[35] A. Celis, M. Jung, X.-Q. Li, and A. Pich, Phys. Lett. B **771**, 168 (2017).
[36] R. Alonso, B. Grinstein, and J. Martin Camalich, Phys. Rev. Lett. **118**, 081802 (2017).
[37] M. Tanabashi *et al.* (Particle Data Group), Phys. Rev. D **98**, 030001 (2018).
[38] S. Fajfer, J. F. Kamenik, I. Nisandzic, and J. Zupan, Phys. Rev. Lett. **109**, 161801 (2012).
[39] Y. Sakaki and H. Tanaka, Phys. Rev. D **87**, 054002 (2013).
[40] M. Tanaka and R. Watanabe, Phys. Rev. D **87**, 034028 (2013).
[41] D. Bečirević, N. Košnik, and A. Tayduganov, Phys. Lett. B **716**, 208 (2012).

[42] A. Datta, M. Duraisamy, and D. Ghosh, Phys. Rev. D **86**, 034027 (2012).
[43] M. Duraisamy and A. Datta, J. High Energy Phys. 09 (2013) 059.
[44] R. Dutta, A. Bhol, and A. K. Giri, Phys. Rev. D **88**, 114023 (2013).
[45] M. Duraisamy, P. Sharma, and A. Datta, Phys. Rev. D **90**, 074013 (2014).
[46] Y. Sakaki, M. Tanaka, A. Tayduganov, and R. Watanabe, Phys. Rev. D **91**, 114028 (2015).
[47] M. Freytsis, Z. Ligeti, and J. T. Ruderman, Phys. Rev. D **92**, 054018 (2015).
[48] R. Alonso, A. Kobach, and J. Martin Camalich, Phys. Rev. D **94**, 094021 (2016).
[49] D. Bardhan, P. Byakti, and D. Ghosh, J. High Energy Phys. 01 (2017) 125.
[50] S. Bhattacharya, S. Nandi, and S. K. Patra, Phys. Rev. D **95**, 075012 (2017).
[51] A. K. Alok, D. Kumar, J. Kumar, S. Kumbhakar, and S. U. Sankar, J. High Energy Phys. 09 (2018) 152.
[52] R. Dutta, arXiv:1710.00351.
[53] A. Azatov, D. Bardhan, D. Ghosh, F. Sgarlata, and E. Venturini, J. High Energy Phys. 11 (2018) 187.
[54] S. Bifani, S. Descotes-Genon, A. Romero Vidal, and M.-H. Schune, J. Phys. G **46**, 023001 (2019).
[55] Z.-R. Huang, Y. Li, C.-D. Lu, M. A. Paracha, and C. Wang, Phys. Rev. D **98**, 095018 (2018).
[56] P. Asadi, M. R. Buckley, and D. Shih, Phys. Rev. D **99**, 035015 (2019).
[57] Q.-Y. Hu, X.-Q. Li, and Y.-D. Yang, arXiv:1810.04939.
[58] F. Feruglio, P. Paradisi, and O. Sumensari, J. High Energy Phys. 11 (2018) 191.
[59] A. Angelescu, D. Bečirević, D. A. Faroughy, and O. Sumensari, J. High Energy Phys. 10 (2018) 183.
[60] S. Iguro, Y. Omura, and M. Takeuchi, arXiv:1810.05843.
[61] S. Bhattacharya, S. Nandi, and S. Kumar Patra, arXiv:1805.08222.
[62] J. Aebischer, J. Kumar, P. Stangl, and D. M. Straub, arXiv:1810.07698.
[63] S. Iguro and Y. Omura, J. High Energy Phys. 05 (2018) 173.
[64] A. Greljo, D. J. Robinson, B. Shakya, and J. Zupan, J. High Energy Phys. 09 (2018) 169.
[65] D. J. Robinson, B. Shakya, and J. Zupan, arXiv:1807.04753.
[66] A. Azatov, D. Barducci, D. Ghosh, D. Marzocca, and L. Ubaldi, J. High Energy Phys. 10 (2018) 092.
[67] M. Jung and D. M. Straub, J. High Energy Phys. 01 (2019) 009.
[68] W. Buchmuller and D. Wyler, Nucl. Phys. **B268**, 621 (1986).
[69] B. Grzadkowski, M. Iskrzynski, M. Misiak, and J. Rosiek, J. High Energy Phys. 10 (2010) 085.
[70] J. Aebischer, A. Crivellin, M. Fael, and C. Greub, J. High Energy Phys. 05 (2016) 037.
[71] M. González-Alonso, J. Martin Camalich, and K. Mimouni, Phys. Lett. B **772**, 777 (2017).
[72] S. S. Gershtein, V. V. Kiselev, A. K. Likhoded, and A. V. Tkabladze, Usp. Fiz. Nauk **165**, 3 (1995) [Phys. Usp. **38**, 1 (1995)].
[73] I. I. Y. Bigi, Phys. Lett. B **371**, 105 (1996).
[74] M. Beneke and G. Buchalla, Phys. Rev. D **53**, 4991 (1996).
[75] C.-H. Chang, S.-L. Chen, T.-F. Feng, and X.-Q. Li, Phys. Rev. D **64**, 014003 (2001).
[76] V. V. Kiselev, A. E. Kovalsky, and A. K. Likhoded, Nucl. Phys. **B585**, 353 (2000).
[77] A. G. Akeroyd and C.-H. Chen, Phys. Rev. D **96**, 075011 (2017).
[78] R. Aaij *et al.* (LHCb Collaboration), J. High Energy Phys. 04 (2013) 001.
[79] V. Khachatryan *et al.* (CMS Collaboration), J. High Energy Phys. 01 (2015) 063.
[80] R. Aaij *et al.* (LHCb Collaboration), Phys. Rev. Lett. **114**, 132001 (2015).
[81] S. Aoki *et al.*, Eur. Phys. J. C **77**, 112 (2017).
[82] C. McNeile, C. T. H. Davies, E. Follana, K. Hornbostel, and G. P. Lepage, Phys. Rev. D **86**, 074503 (2012).
[83] A. Datta, S. Kamali, S. Meinel, and A. Rashed, J. High Energy Phys. 08 (2017) 131.
[84] F. U. Bernlochner, Z. Ligeti, D. J. Robinson, and W. L. Sutcliffe, Phys. Rev. Lett. **121**, 202001 (2018).
[85] S. Descotes-Genon, L. Hofer, J. Matias, and J. Virto, J. High Energy Phys. 06 (2016) 092.
[86] R. Alonso, B. Grinstein, and J. Martin Camalich, J. High Energy Phys. 10 (2015) 184.
[87] L. Calibbi, A. Crivellin, and T. Ota, Phys. Rev. Lett. **115**, 181801 (2015).
[88] S. Fajfer and N. Košnik, Phys. Lett. B **755**, 270 (2016).
[89] R. Barbieri, G. Isidori, A. Pattori, and F. Senia, Eur. Phys. J. C **76**, 67 (2016).
[90] R. Barbieri, C. W. Murphy, and F. Senia, Eur. Phys. J. C **77**, 8 (2017).
[91] G. Hiller, D. Loose, and K. Schonwald, J. High Energy Phys. 12 (2016) 027.
[92] B. Bhattacharya, A. Datta, J.-P. Guévin, D. London, and R. Watanabe, J. High Energy Phys. 01 (2017) 015.
[93] D. Buttazzo, A. Greljo, G. Isidori, and D. Marzocca, J. High Energy Phys. 11 (2017) 044.
[94] J. Kumar, D. London, and R. Watanabe, Phys. Rev. D **99**, 015007 (2019).
[95] N. Assad, B. Fornal, and B. Grinstein, Phys. Lett. B **777**, 324 (2018).
[96] L. Di Luzio, A. Greljo, and M. Nardecchia, Phys. Rev. D **96**, 115011 (2017).
[97] L. Calibbi, A. Crivellin, and T. Li, Phys. Rev. D **98**, 115002 (2018).
[98] M. Bordone, C. Cornella, J. Fuentes-Martin, and G. Isidori, Phys. Lett. B **779**, 317 (2018).
[99] R. Barbieri and A. Tesi, Eur. Phys. J. C **78**, 193 (2018).
[100] M. Blanke and A. Crivellin, Phys. Rev. Lett. **121**, 011801 (2018).
[101] A. Greljo and B. A. Stefanek, Phys. Lett. B **782**, 131 (2018).
[102] M. Bordone, C. Cornella, J. Fuentes-Martín, and G. Isidori, J. High Energy Phys. 10 (2018) 148.
[103] S. Matsuzaki, K. Nishiwaki, and K. Yamamoto, J. High Energy Phys. 11 (2018) 164.
[104] A. Crivellin, C. Greub, F. Saturnino, and D. Muller, Phys. Rev. Lett. **122**, 011805 (2019).
[105] L. Di Luzio, J. Fuentes-Martin, A. Greljo, M. Nardecchia, and S. Renner, J. High Energy Phys. 11 (2018) 081.

[106] A. Biswas, D. Kumar Ghosh, N. Ghosh, A. Shaw, and A. K. Swain, arXiv:1808.04169.
[107] N. G. Deshpande and A. Menon, J. High Energy Phys. 01 (2013) 025.
[108] Y. Sakaki, M. Tanaka, A. Tayduganov, and R. Watanabe, Phys. Rev. D **88**, 094012 (2013).
[109] M. Bauer and M. Neubert, Phys. Rev. Lett. **116**, 141802 (2016).
[110] Y. Cai, J. Gargalionis, M. A. Schmidt, and R. R. Volkas, J. High Energy Phys. 10 (2017) 047.
[111] A. Crivellin, D. Muller, and T. Ota, J. High Energy Phys. 09 (2017) 040.
[112] W. Altmannshofer, P. Bhupal Dev, and A. Soni, Phys. Rev. D **96**, 095010 (2017).
[113] D. Marzocca, J. High Energy Phys. 07 (2018) 121.
[114] X.-G. He and G. Valencia, Phys. Rev. D **87**, 014014 (2013).
[115] A. Greljo, G. Isidori, and D. Marzocca, J. High Energy Phys. 07 (2015) 142.
[116] S. M. Boucenna, A. Celis, J. Fuentes-Martin, A. Vicente, and J. Virto, Phys. Lett. B **760**, 214 (2016).
[117] X.-G. He and G. Valencia, Phys. Lett. B **779**, 52 (2018).
[118] J. Kalinowski, Phys. Lett. B **245**, 201 (1990).
[119] W.-S. Hou, Phys. Rev. D **48**, 2342 (1993).
[120] N. Kosnik, Phys. Rev. D **86**, 055004 (2012).
[121] A. Biswas, A. Shaw, and A. K. Swain, arXiv:1811.08887.
[122] A. Crivellin, C. Greub, and A. Kokulu, Phys. Rev. D **86**, 054014 (2012).
[123] A. Crivellin, A. Kokulu, and C. Greub, Phys. Rev. D **87**, 094031 (2013).
[124] A. Celis, M. Jung, X.-Q. Li, and A. Pich, J. High Energy Phys. 01 (2013) 054.
[125] P. Ko, Y. Omura, and C. Yu, J. High Energy Phys. 03 (2013) 151.
[126] A. Crivellin, J. Heeck, and P. Stoffer, Phys. Rev. Lett. **116**, 081801 (2016).
[127] L. Dhargyal, Phys. Rev. D **93**, 115009 (2016).
[128] C.-H. Chen and T. Nomura, Eur. Phys. J. C **77**, 631 (2017).
[129] S. Iguro and K. Tobe, Nucl. Phys. **B925**, 560 (2017).
[130] R. Martinez, C. F. Sierra, and G. Valencia, Phys. Rev. D **98**, 115012 (2018).
[131] A. Biswas, D. K. Ghosh, A. Shaw, and S. K. Patra, arXiv:1801.03375.
[132] D. Bečirević, S. Fajfer, N. Košnik, and O. Sumensari, Phys. Rev. D **94**, 115021 (2016).
[133] D. Bečirević, I. Doršner, S. Fajfer, N. Košnik, D. A. Faroughy, and O. Sumensari, Phys. Rev. D **98**, 055003 (2018).
[134] R. Alonso, E. E. Jenkins, A. V. Manohar, and M. Trott, J. High Energy Phys. 04 (2014) 159.
[135] S. Iguro, T. Kitahara, Y. Omura, R. Watanabe, and K. Yamamoto, J. High Energy Phys. 02 (2019) 194.
[136] A. Greljo, J. Martin Camalich, and J. D. Ruiz-Álvarez, arXiv:1811.07920.
[137] A. Greljo, *B* anomalies vs high-p_T lepton tails, in *Workshop on High-Energy Implications of Flavor Anomalies* (CERN, 2018), https://indico.cern.ch/event/701759/contributions/3168372/attachments/1739898/2815060/CERN-Tails-2018.pdf.